J. Fluid Mech. (2002), *vol.* 462, *pp.* 161–183.
DOI: 10.1017/S0022112002008522 Printed in the United Kingdom

Double-diffusive finger convection: influence of concentration at fixed buoyancy ratio

By SCOTT E. PRINGLE[1,2] AND ROBERT J. GLASS[1]

[1]Flow Visualization and Processes Laboratory, Sandia National Laboratories, Albuquerque, NM, USA

[2]School of Engineering, Department of Civil Engineering, University of New Mexico, Albuquerque, NM, USA

(Received 16 February 2001 and in revised form 3 January 2002)

Double-diffusive finger convection is studied experimentally in a transparent Hele-Shaw cell for a two-solute system. A less dense sucrose solution is layered on top of a more dense salt solution using a laminar flow technique, and convective motion is followed photographically from the static state. We systematically increase solute concentrations from dilute to the solubility limit of the salt solution while maintaining a fixed buoyancy ratio of approximately 1.08. Across the 14 experiments conducted, the convective motion shows considerable variation in both structure and time scale. We find that new finger pairs form continuously within a finger generation zone where complexity increases with Rayleigh number, reaches a peak, and then decreases for highly concentrated solutions. The vertical finger length scale grows linearly in time across the full concentration range. The vertical finger velocity also increases linearly with Rayleigh number, but as the concentrations increase, deviation from linearity and asymmetrical convection occur. The horizontal length scale grows as a power law in time with the exponent constant over most of the range; again, deviations are observed for highly concentrated solutions. The observed deviations at high concentrations are attributed to the increasing nonlinearity in the governing equations as the solutions approach their solubility limits. There, the fluid properties become functions of solute concentration and vary significantly within the experimental fields suppressing structural complexity, imparting asymmetry to the convective motion, and influencing emergent vertical and horizontal length scales and their growth.

1. Introduction

The dissimilar diffusion of density affecting components such as solutes and heat can create structure and drive convective motion at a wide variety of scales across a diverse set of fluid applications (see reviews by Turner 1985; Nield & Bejan 1992). This motion has been termed double-diffusive convection (2 components) or multi-component convection (3 or more components) with examples ranging from the mixing of stellar gases (e.g. Spiegel 1972; Proctor & Weiss 1982; Loper & Roberts 1983) to the solidification of melts and pattern formation in crystal growth (e.g. Langer 1980; Azouni 1981; Fisher 1981). Double-diffusive convection has been studied most extensively in oceanography (e.g. Gregg 1973; Stern 1975; Schmitt 1994) where the heat–salt fingering mechanism operating on a scale of centimetres can affect ocean dynamics and circulation over scales of many kilometres. Within porous media and in the context of environmental problems, it is also possible that this mechanism

can lead to surface–groundwater interactions and influence subsurface contaminant transport (Green 1984; Imhoff & Green 1988; Cooper, Glass & Tyler 1997).

In the traditional analysis of the double-diffusive system, the dimensionless forms of the conservation equations for momentum and mass yield two independent dimensionless parameters: the Rayleigh number for the faster diffusing component (T), $R_T = (\beta_T \Delta T g H^3 / D_T \nu)$, and the Rayleigh number for the slower diffusing component (S), $R_S = (\beta_S \Delta S g H^3 / D_T \nu)$, where β_T and β_S are the chemical expansion coefficients, ΔT and ΔS are characteristic concentration differences, H is a characteristic distance, g is the acceleration due to gravity, D_T is the molecular diffusion coefficient of the faster diffusing component, and ν is the average fluid kinematic viscosity. The dimensionless forms of the two advection–diffusion equations yield an additional dimensionless parameter, $\tau = D_S / D_T$, where D_S is the molecular diffusion coefficient of the slower diffusing component. In a large portion of the literature, it has been common to consider behaviour as a function of only the buoyancy ratio, $R_\rho = (R_T / R_S) = (\beta_T \Delta T / \beta_S \Delta S)$. However, a dependency on the magnitude of solute concentrations (i.e. R_T and R_S) will exist beyond their simple ratio embodied in R_ρ, as has been pointed out by recent experiments and numerical simulations (e.g. Taylor & Veronis 1996; Shen & Veronis 1997).

In this paper, we focus on the two-solute system and consider the dependency of double-diffusive finger convection on the magnitude of solute concentrations (and corresponding Rayleigh numbers) while maintaining a fixed R_ρ. The components considered are two miscible solutes, sodium chloride (salt) and sucrose, having a factor of ~ 3 difference in molecular diffusion coefficients. Within a transparent Hele-Shaw cell, an initial condition was formed yielding two horizontal fluid layers, sucrose on top of salt, with a stabilizing, near step function, density distribution. We systematically increased the component concentrations from very dilute to the solubility limit of the salt while maintaining a fixed R_ρ of ~ 1.08. Because of the increase in solution viscosity at high concentration, Rayleigh numbers reach an apex and then begin to decrease with further increases in concentration along the R_ρ line in Rayleigh space. In this region of high concentration, we find Rayleigh numbers to non-uniquely define convective behaviour.

For all but the most dilute experiment, a self-organized, horizontal array of vertically convecting fingers develops. The appearance of the convecting structure varies with Rayleigh number from a few wide fingers with diffuse edges and relatively low growth rates, to a large number of thin and distinct fingers with high growth rates. In general, we found new finger pairs to form throughout an experiment within a finger generation zone that straddles the initial contact between the two miscible fluids. The overall structural complexity of the fingering fields systematically increases with Rayleigh number over most of the range tested. However, for highly concentrated solutions, vertical growth becomes asymmetric, and where Rayleigh numbers decrease relative to the apex, structural complexity is suppressed. Measurement of the emergent vertical and horizontal length scales of the convecting field in time for a given experiment shows linear and power law behaviour, respectively. Across the experimental series, the vertical finger velocity first varies linearly with Rayleigh number and then becomes constant for more concentrated solutions. The exponent that defines the power law growth of the horizontal length scale first is constant with Rayleigh number at a value of ~ 0.5 and then decreases for highly concentrated solutions. In addition, the early time horizontal length scale decreases with Rayleigh number to the -0.5 power as suggested by theory and then becomes constant at higher solution concentrations. These experimental results underline the statements

by Taylor & Veronis (1996) that double-diffusive convection cannot be treated as a single phenomenon or characterized by a single analysis, especially when considering solute systems.

2. Theory

In support of our experimental design, we consider the traditional governing equations, assumptions, and dimensionless control parameters as follows. The problem of interest consists of two uniform, horizontal layers composed of solutions containing T and S separated by a miscible interface within a Hele-Shaw cell of permeability k and vertical extent H. The lower (denser) layer contains the more rapidly diffusing component at concentration T, and the upper (lighter) layer contains the slower diffusing component at concentration S. Cartesian coordinates are defined with the origin at the lower boundary and $z = H$ at the upper boundary of the cell. For convection to occur, the fluid density must be a function of the concentration such as expressed in the following equation of state,

$$\rho = \rho_0(1 + \beta_T T + \beta_S S), \tag{1}$$

where ρ_0 is the reference density of pure water, $\beta_T = (1/\rho_0)(\partial\rho/\partial T)$, and $\beta_S = (1/\rho_0)(\partial\rho/\partial S)$ are the chemical expansion coefficients.

In the standard theoretical development, it is assumed that the Oberbeck–Boussinesq approximation holds, that is, variations in density are retained only in the buoyant term of the momentum equation. Additionally, concentration variations must have negligible effects on component diffusion coefficients, chemical expansion coefficients and fluid viscosities within the problem domain. With these constraints, the governing equations of conservation of mass, Darcy momentum, and advection–diffusion for each component are

$$\nabla \cdot \boldsymbol{V} = 0, \tag{2}$$

$$\boldsymbol{V} = -\frac{k}{\mu}(\nabla P + \rho \boldsymbol{g}), \tag{3}$$

$$\phi\left(\frac{\partial T}{\partial t}\right) + \boldsymbol{V} \cdot \nabla T = D_T(\nabla^2 T), \tag{4}$$

$$\phi\left(\frac{\partial S}{\partial t}\right) + \boldsymbol{V} \cdot \nabla S = D_S(\nabla^2 S), \tag{5}$$

where $\boldsymbol{V}$, k, μ, P, ρ, $\boldsymbol{g}$, ϕ, t and D are, respectively, the velocity vector, intrinsic permeability, dynamic viscosity, pressure, fluid density, the vector of acceleration due to gravity within the plane of the cell (positive downward and modified for the inclination of the cell), porous media porosity, time, and diffusion coefficient, with $\nabla = ((\partial/\partial x)\hat{\boldsymbol{i}} + (\partial/\partial y)\hat{\boldsymbol{j}} + (\partial/\partial z)\hat{\boldsymbol{k}})$, $\nabla^2 = ((\partial^2/\partial x^2) + (\partial^2/\partial y^2) + (\partial^2/\partial z^2))$, and $\hat{\boldsymbol{i}}$, $\hat{\boldsymbol{j}}$, $\hat{\boldsymbol{k}}$ the unit vectors in the x-, y-, z-directions. Combining equations (1), (2) and (3), (i.e. substituting (1) into (3), taking the curl of (3) twice, and imposing (2)) results in the following momentum equation

$$\nabla^2 \boldsymbol{V} = \left(\frac{kg}{\nu}\right)\left(\beta_T\left(-\frac{\partial^2 T}{\partial x \partial z}\hat{\boldsymbol{i}} - \frac{\partial^2 T}{\partial y \partial z}\hat{\boldsymbol{j}} + (\nabla^2_{xy} T)\hat{\boldsymbol{k}}\right) + \beta_S\left(-\frac{\partial^2 S}{\partial x \partial z}\hat{\boldsymbol{i}} - \frac{\partial^2 S}{\partial y \partial z}\hat{\boldsymbol{j}} + (\nabla^2_{xy} S)\hat{\boldsymbol{k}}\right)\right), \tag{6}$$

where $\nu = \mu/\rho_0$ is the average kinematic viscosity and $\nabla^2_{xy} = (\partial^2/\partial x^2) + (\partial^2/\partial y^2)$.

The dimensionless forms (Nield & Bejan 1992) of equations (4) to (6) can be written as

$$\nabla^2 \boldsymbol{V}^* = R_T \left(-\frac{\partial^2 T^*}{\partial x^* \partial z^*} \hat{\boldsymbol{i}} - \frac{\partial^2 T^*}{\partial y^* \partial z^*} \hat{\boldsymbol{j}} + \nabla^2_{xy} T^* \hat{\boldsymbol{k}} \right) + R_S \left(-\frac{\partial^2 S^*}{\partial x^* \partial z^*} \hat{\boldsymbol{i}} - \frac{\partial^2 S^*}{\partial y^* \partial z^*} \hat{\boldsymbol{j}} + \nabla^2_{xy} S^* \hat{\boldsymbol{k}} \right), \tag{7}$$

$$\phi \frac{\partial T^*}{\partial t^*} + \boldsymbol{V}^* \cdot \nabla T^* = \nabla^2 T^*, \tag{8}$$

$$\phi \frac{\partial S^*}{\partial t^*} + \boldsymbol{V}^* \cdot \nabla S^* = \tau \nabla^2 S^*, \tag{9}$$

where all starred quantities may be dimensionalized using the following scales: H for the length scale, H^2/D_T for the time scale, D_T/H for the velocity scale, and the maximum problem concentrations ΔT and ΔS for the concentration scales. The dimensionless diffusivity ratio is given as in the general fluid problem by $\tau = D_S/D_T$; however, the dimensionless Rayleigh numbers for the Hele-Shaw problem are slightly different. In the Hele-Shaw problem, the cell permeability is used to scale viscous influences yielding $R_T = (\beta_T \Delta T g H k / D_T \nu)$ and $R_S = (\beta_S \Delta S g H k / D_T \nu)$. Based on our problem, with sugar overlying salt, the signs of R_T and R_S are negative and positive, respectively. For this set of equations, Nield (1968) has determined the stability boundary for double-diffusive fingering as

$$R_T + (R_S/\tau) = R_c, \tag{10}$$

where $0 \leqslant R_c \leqslant 4\pi^2$, depending on system boundary conditions. This relation forms a straight line in Rayleigh space above which convection occurs.

In search of a single characteristic control parameter, often R_T and R_S are combined to yield the dimensionless buoyancy ratio, R_ρ, as

$$R_\rho = \frac{R_T}{R_S} = \frac{\beta_T \Delta T}{\beta_S \Delta S}. \tag{11}$$

with reference to (7), R_ρ essentially weighs the relative importance of the T and S terms on its right-hand side and is negative for our sucrose over salt problem. Arbitrarily choosing to eliminate R_T, we may express the momentum equation (7) and the stability boundary (10) in terms of R_ρ and R_S as

$$\frac{1}{R_S} \nabla^2 \boldsymbol{V}^* = R_\rho \left(-\frac{\partial^2 T^*}{\partial x^* \partial z^*} \hat{\boldsymbol{i}} - \frac{\partial^2 T^*}{\partial y^* \partial z^*} \hat{\boldsymbol{j}} + \nabla^2_{xy} T^* \hat{\boldsymbol{k}} \right) + \left(-\frac{\partial^2 S^*}{\partial x^* \partial z^*} \hat{\boldsymbol{i}} - \frac{\partial^2 S^*}{\partial y^* \partial z^*} \hat{\boldsymbol{j}} + \nabla^2_{xy} S^* \hat{\boldsymbol{k}} \right), \tag{12}$$

and

$$\left(\frac{R_c}{R_S} - R_\rho \right) = \tau^{-1}. \tag{13}$$

Thus, for large R_S or $R_c = 0$, stability is dependent on only R_ρ, as has been verified experimentally by Cooper *et al.* (1997), while the determination of post instability behaviour requires the additional knowledge of R_T or R_S.

At high component concentrations, the diffusion coefficients, chemical expansion coefficients and fluid viscosities will all vary significantly within the problem domain,

and thus the development above will no longer strictly apply. Equations for fluid momentum (3) and the advection–diffusion of each component, (4) and (5), become nonlinear and the definition of appropriate dimensionless control parameters becomes somewhat ambiguous. In our experimental design detailed below, we will consider the variation in system behaviour at a single fixed R_ρ for the full range of concentrations from dilute to near the solubility limits in a two-component solute system. In this manner, R_S, R_T, and τ will vary systematically and the nonlinearity within the governing equations will naturally increase as we move to high solute concentrations.

3. Experimental design

Our objective is to study the behaviour of double-diffusive finger convection at fixed R_ρ as we systematically increase component concentrations and allow the dimensionless parameters R_S, R_T and τ to vary. We define system behaviour based on the evolving structure of the concentration field and quantify this behaviour with corresponding measures of emergent vertical and horizontal length scales in time. This structure can be clearly visualized and recorded photographically using a transparent Hele-Shaw (parallel plate) flow cell in combination with a dye added to one of the solutions. As have many other studies in the past, we choose the two-component sodium chloride (T) and sucrose (S) system, yielding a factor of ~ 3 difference in the molecular diffusion coefficients at dilute concentrations. The initial condition is formed with a layer of less dense sucrose solution above a layer of more dense and dyed sodium chloride (salt) solution. To be far from diffusive stability, R_ρ is controlled at 1.083 (close to neutral buoyancy) as we systematically increase the salt and sucrose concentrations in the lower and upper solutions, respectively, from dilute ($< 0.1\%$ solute by mass) to very concentrated ($\sim 35\%$ by mass for salt which is near its solubility limit and $\sim 70\%$ by mass for sucrose).

Table 1 presents the parameters for each of the 14 experiments conducted. Our design roughly doubled the solution concentrations for each successive experiment, with slight adjustment for variation in expansion coefficients with concentration to maintain the target R_ρ. The chemical expansion coefficients (β_T, β_S) are calculated based on linear regression of the density–concentration data from Weast (1986) between zero and the initial concentration of each solution. The molecular diffusion coefficients (D_T, D_S) are obtained from Stokes (1950) and Irani & Adamson (1958), respectively, at 50% of the maximum concentration representing the average concentration of each solution within the initial fluid interface. The viscosities (v_T, v_S), based on the solution concentrations, are obtained from Weast (1986). As we show in figure 1, over most of the range of concentrations considered, diffusion coefficients ($\tau \sim 0.3$) and fluid viscosities are nearly constant. However, at high concentrations, D_S decreases (τ approaches ~ 0.2), while the viscosity of each fluid increases significantly (sucrose more than salt). The error in the fluid properties is estimated to be $\sim 2\%$.

Figure 2 shows the locations of the 14 experimental points in Rayleigh space as defined by initial conditions and with H taken as the vertical height of the flow cell (16.25 cm). As is common in the literature, we have defined R_T and R_S here and in the remainder of the paper with the average viscosity of the fluid (average of v_T and v_S in table 1). The experimental transect starts out as a 'spoke' emanating from the origin (figure 2*a*) and as concentrations increase (figure 2*b*), it reaches an apex in Rayleigh space (experiment 12), and then reverses direction (experiments 13 and 14). Note, for experiments 11, 13 and 14, slight deviation ($\sim 1\%$) from the target R_ρ of 1.083 occurred, as can be seen in figure 2(*b*).

Experiment	Symbol identifier	β_T	β_S	$-\Delta T$ (kg kg^{-1})	ΔS (kg kg^{-1})	$D_T \times 10^9$ (m^2 s^{-1})	$D_S \times 10^{10}$ (m^2 s^{-1})	$v_T \times 10^6$ (m^2 s^{-1})	$v_S \times 10^6$ (m^2 s^{-1})	$-R_\rho$	$-R_T$	R_S
1	⊡	0.7268	0.3846	0.0002184	0.0003813	1.61	5.05	1.01	1.04	1.082 ± 0.008	385 ± 12	355 ± 11
2	⊞	0.7268	0.3846	0.0004369	0.0007625	1.60	5.05	1.01	1.04	1.083 ± 0.008	772 ± 23	713 ± 21
3	▼	0.7268	0.3846	0.0007646	0.0013345	1.59	5.05	1.01	1.04	1.083 ± 0.008	1357 ± 41	1253 ± 38
4	▲	0.7268	0.3846	0.0010923	0.0019063	1.59	5.05	1.01	1.04	1.083 ± 0.008	1946 ± 58	1798 ± 54
5	◆	0.7268	0.3846	0.0017475	0.0030500	1.57	5.05	1.01	1.04	1.083 ± 0.008	3139 ± 94	2899 ± 87
6	■	0.7268	0.3846	0.0034950	0.0061052	1.54	5.04	1.01	1.05	1.082 ± 0.008	6395 ± 192	5912 ± 177
7	●	0.7119	0.3815	0.0068130	0.0117400	1.50	5.02	1.01	1.06	1.083 ± 0.008	12 494 ± 375	11 537 ± 346
8	△	0.7000	0.3790	0.0103080	0.0175800	1.48	5.00	1.02	1.06	1.083 ± 0.008	18 696 ± 561	17 265 ± 518
9	+	0.7009	0.3786	0.0137145	0.0234400	1.48	4.98	1.02	1.07	1.083 ± 0.008	24 814 ± 744	22 909 ± 687
10	×	0.6901	0.3705	0.0361360	0.0621500	1.48	4.85	1.03	1.15	1.083 ± 0.008	61 880 ± 1856	57 139 ± 1714
11	◇	0.6735	0.3569	0.0722720	0.1264783	1.47	4.63	1.07	1.31	1.078 ± 0.008	110 910 ± 3327	102 849 ± 3085
12	□	0.6460	0.3320	0.1441103	0.2588000	1.49	4.22	1.16	1.84	1.083 ± 0.008	166 086 ± 4983	153 408 ± 4602
13	○	0.5978	0.2808	0.3150000	0.6250000	1.53	3.19	1.54	4.62	1.073 ± 0.008	159 168 ± 4775	148 329 ± 4450
14	▽	0.5877	0.2745	0.3500000	0.7000000	1.54	3.00	1.64	5.43	1.071 ± 0.008	150 559 ± 4517	140 633 ± 4219

TABLE 1. Summary of parameters for the series of experiments conducted. All values represent initial conditions. β_T, β_S ($\pm$0.5%) are the chemical expansion coefficients for sodium chloride and sucrose, respectively, calculated based on linear regression of the density-concentration data from Weast (1986) between zero and the initial concentration of the fluid layer. ΔT and ΔS ($\pm$0.002%) are the maximum concentrations of sodium chloride and sucrose, respectively. D_T and D_S ($\pm$2%) are the molecular diffusion coefficients of sodium chloride taken from Stokes (1950) and sucrose from Irani & Adamson (1958) at 50% of the maximum concentration representing the average of each solution. v_T and v_S ($\pm$2%) are the kinematic viscosities for sodium chloride and sucrose, respectively, taken from Weast (1986) for the initial solution concentrations. R_ρ is the buoyancy ratio defined as $\beta_T \Delta T / \beta_S \Delta S$. Note, R_ρ value for experiments 11, 13 and 14 deviate slightly from the target value of 1.083. R_T ($= \beta_T \Delta T g H k / D_T v$), $\pm$3%, is the salinity Rayleigh number, and H is defined as the height of the cell, 16.25 cm. R_S ($= \beta_S \Delta S g H k / D_T v$), $\pm$3%, is the sucrose Rayleigh number. g (acceleration due to gravity) is modified by $\cos(\theta)$ where θ is the angle of the cell from the vertical (35°). k is the intrinsic permeability of the cell given as 3.058×10^{-9} m^2.

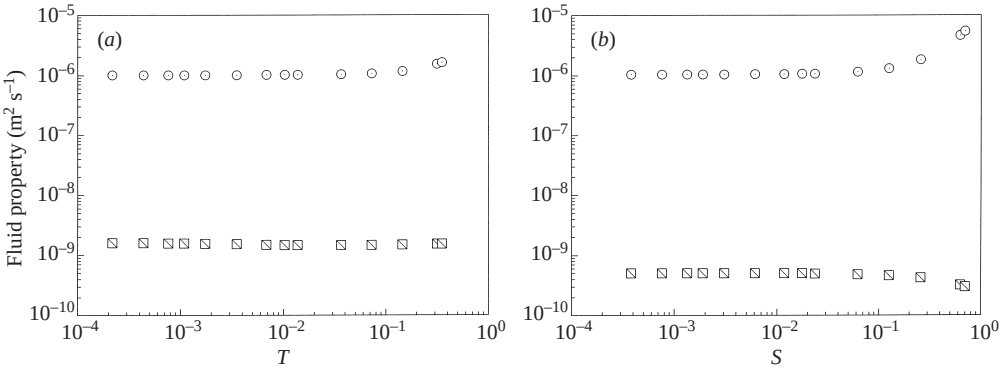

FIGURE 1. Variability in the fluid properties of ⧅, diffusivity and ⊙, viscosity with increase in (*a*) salt concentration (T kg kg^{-1}) and (*b*) sucrose concentration (S kg kg^{-1}).

With reference to (12), we require only specification of a single Rayleigh number as the other is given by (11). The choice of which Rayleigh number, R_T or R_S, to use is subjective. The choice of R_S can be justified because sucrose is the destabilizing component of the system; however, the use of R_T can be justified because salt is the faster diffusing solute and can be viewed as the component contributing the most to the local density difference. In the remainder of the paper we have arbitrarily chosen to consider system behaviour as a function of R_S.

The Hele-Shaw cell used for all experiments (internal dimensions: 30.51 cm wide × 16.25 cm high with a 0.0192 cm gap) was fabricated from two flat glass plates each mounted on a rectangular metal frame. A clear rigid shim was placed on each long edge of the bottom glass plate, and the cell was assembled by placing the top plate in contact with the shims and bolting the frames together. The cell was sealed along the remaining two sides and placed in a clamp that maintained the cell at an angle of 35° from the vertical. The intrinsic permeability of the cell was measured to be 3.058×10^{-9} m^2, with negligible change from the beginning to the end of the experimental series.

The most common method applied to obtain an initial horizontal layering of two solutions uses a physical barrier placed within the cell gap that is removed to bring the two solutions into contact (e.g. Wooding 1969; Taylor & Veronis 1986; Cooper *et al.* 1997, 2001). However, removal of the barrier at the start of an experiment causes significant initial disturbances leading to ambiguity in the interpretation of system behaviour (e.g. Linden, Redondo & Youngs 1994; Dalziel, Linden & Youngs 1999). To avoid these disturbances, we developed a layering method that does not employ a physical barrier. The solutions enter a water-saturated cell at the upper and lower corners of one side and exit at the midpoint between the corners of the other (see figure 3*a*). The pressure at each entry and exit point is controlled to yield a nearly flat, horizontal, undisturbed miscible interface of the order of 1 mm thick. In this configuration, over 100 cell volumes of each solution are flushed to assure concentration uniformity above and below the interface and yield a consistent and reproducible initial condition for each of the 14 experiments. Quantitative light transmission techniques (e.g. Detwiler, Rajaram & Glass 2000) were applied in preliminary experiments to verify that the experimental procedure yielded the specified initial condition.

Once the initial condition was established, flow valves connected to the source and sink were closed, and the initially static system was allowed to evolve naturally. We

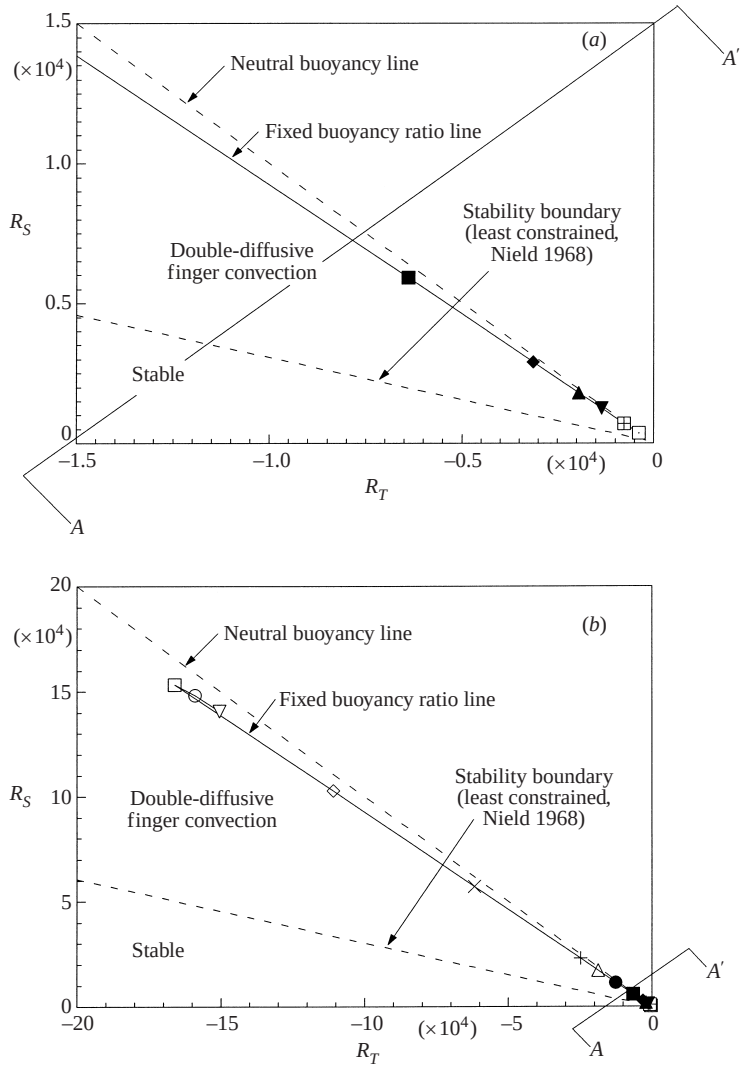

FIGURE 2. Location of experimental points in Rayleigh space for a fixed R_ρ of 1.083 (tolerance within 1%). (*a*) The low magnitude Rayleigh number space with experimental locations 1 to 6. (*b*) The full Rayleigh space region of interest with experimental points 6 to 14 clearly defined. ⊡ experiment 1; ⊞, 2; ▼, 3; ▲, 4; ◆, 5; ■, 6; ●, 7; △, 8; +, 9; ×, 10; ◇, 11; □, 12; ○, 13, ▽, 14.

tagged the salt solution with a passive dye tracer at a concentration of $1\,\mathrm{g\,l^{-1}}$ (Warner Jenkins FD&C Blue #1). The addition of the dye has a negligible influence on fluid density and allows us to distinguish between the two fluids during the course of an experiment. The evolution of the convection was recorded using a 35 mm camera at predetermined time increments with a diffuse fluorescent light source backlighting the entire flow field (figure 3*b*). The system was located in a controlled temperature environment ($20.8\,^\circ\mathrm{C} \pm 0.3\,^\circ\mathrm{C}$) and the bulbs were energized for a 1 min period before a photograph was taken and then immediately turned off to minimize thermal loading. We note that while the diffusivity of the dye was 0.4 times that of the salt that it tagged, convection far exceeded diffusion in all but the most dilute experiment and

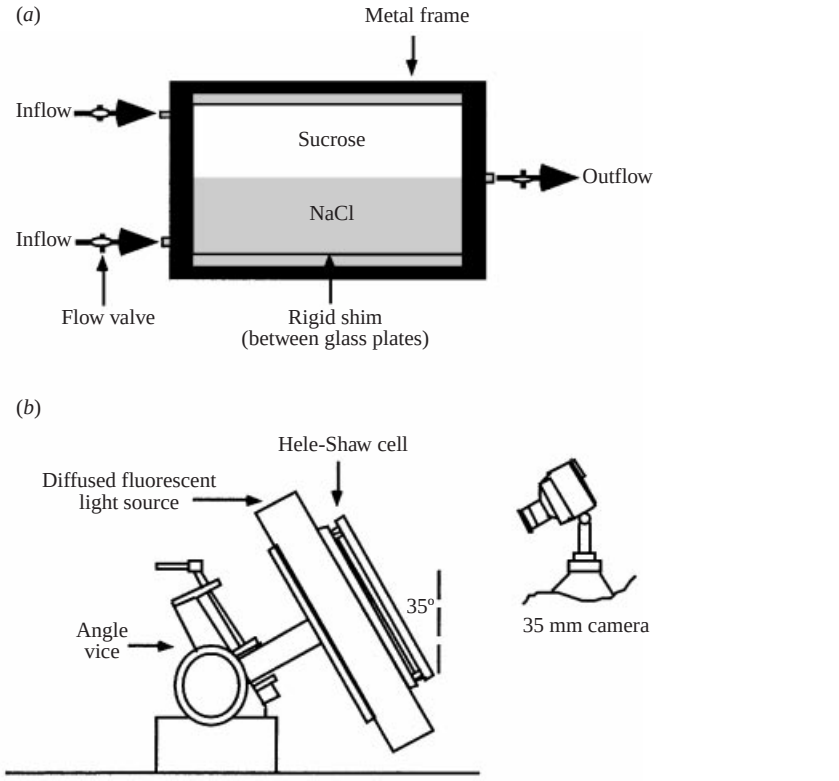

FIGURE 3. Schematic of the Hele-Shaw cell and the experimental apparatus. (*a*) Configuration of the two solutions (less dense sucrose solution over more dense salt solution) within the Hele-Shaw cell of flow dimensions $30.51 \times 16.25\,\mathrm{cm}^2$ with 0.0192 cm gap. For all experiments, the Hele-Shaw cell was orientated at 35° from vertical. The solutions enter a water-saturated cell at the upper and lower corners of the left-hand side and exit at the midpoint between the corners of the right-hand side. The pressure at each entry and exit point is controlled to yield a nearly flat horizontal undisturbed miscible interface of the order of 1 mm thick without the use of a physical barrier. (*b*) A diffused fluorescent light source backlights the entire flow field, and a 35 mm camera is used to photograph the convective motion.

thus measures of the emergent length scales based on the dye fields should accurately represent those of the underlying salt and sucrose.

Finally, to consider the intrinsic variability of the resulting convection for a single experimental point, and to understand how this variability affects our interpretation of behavioural differences across the experimental series, experiment 9 was repeated 4 additional times. The overall finger structures in each of the five runs are nearly indistinguishable; however, as we would expect, fingers form at different locations in each run. Results indicate that the representative variability of the measured length scales at a given experimental point is negligible compared to the variation observed with R_S.

4. Results and discussion

Across the 14 experiments, the evolving concentration fields show marked differences in both emergent structure and evolution rate. To illustrate these differences, we present one photograph each from 8 of the 14 experiments taken just before the

fastest convecting fingers have reached either the top or bottom boundary (figure 4). In general, as R_S increases by nearly three orders of magnitude, fingers narrow and their velocities increase. Figure 5 shows the time, t^*_{top} ($= t_{top}D_t/H^2$), for experiments 2 to 14, and figure 6 the horizontal length scale, λ^*_{top} ($= \lambda_{top}/H$), just prior to finger contact with the top or bottom boundary. λ_{top} was measured by dividing the cell width by half the number of transitions from dyed to undyed solution at the location of the initial fluid interface (experiments 2 to 12). Figure 6 includes data only for experiments 2 to 12 because the fineness of the structure at the initial fluid interface did not allow us to count transitions with certainty for experiments 13 or 14. The time to reach the top or bottom boundary follows an approximate power law (exponent of -1.6) over most of the range, but deviates at high R_S. For the horizontal length scale, we also see power law behaviour (exponent of -0.6). We note, in figure 4 (f–h), that at high R_S, the convection becomes asymmetric about the initial fluid interface, as shown in figure 7. In the following sections, we first discuss the trends in qualitative system behaviour as Rayleigh numbers vary. We then present quantitative measurements of emergent vertical and horizontal length scales as a function of time and R_S.

4.1. *Qualitative description*

In the first experiment, $R_S = 355$ (figure 4a), it is difficult to detect convection by eye although there appears to be a low-amplitude, large-wavelength anomaly in the middle and at either end of the cell. Across all of the higher R_S experiments, fingers form a regular array at the initial fluid interface and grow, eventually reaching the top and bottom of the cell. However, soon after initiation, the convective motion undergoes a transition where new finger pairs are generated from a zone straddling the location of the initial fluid interface, termed the 'finger generation' zone by Cooper *et al.* (2001). There, new fingers are generated throughout the course of each experiment. Figure 8 compares a portion of an early time photograph (figure 8a) with two later times for R_S of 2.29×10^4 (figure 4e). Wide fluid 'trunks' that are rooted within the generation zone (wider dark and light regions in figure 8b, c) feed growing fingers, become unstable, and generate new finger pairs. This behaviour is consistent with the numerical simulations of Shen & Veronis (1991) and is attributed to the intrinsically unstable vertical density contrast across the inclined trunk edges. The new finger pairs generated (one in the middle, one on the left and one on the right in figure 8c) have similar vertical and horizontal scales to the dominant fingers at earlier time (figure 8b). There is a tendency for these newly formed fingers to become entrained within the core of previous fingers and follow along tracks or 'conduits' such as described by Cooper *et al.* (2001). This entrainment process leads to the formation of a local stair-step concentration profile along the conduit. As R_S and, hence, finger velocities increase, the finger shape changes from wide and diffuse

FIGURE 4. Series of eight photographs showing the evolved concentration fields just prior to contact between the fastest convecting finger and either the top or bottom boundary. Sucrose solution is denoted by the lighter regions and salt solution by the darker regions. The sucrose Rayleigh number and the elapsed time of convection for each experiment are defined as: (a) experiment 1: $R_S = 355$ at $t = 425$ h; (b) experiment 3: $R_S = 1253$ at $t = 140$ h; (c) experiment 5: $R_S = 2899$ at $t = 36$ h; (d) experiment 7: $R_S = 11\,537$ at $t = 3$ h; (e) experiment 9: $R_S = 22\,909$ at $t = 1.3$ h; (f) experiment 11: $R_S = 102\,849$ at $t = 0.35$ h; (g) experiment 12: $R_S = 153\,408$ at $t = 0.35$ h; (h) experiment 14: $R_S = 140\,633$ at $t = 0.35$ h. The concentration of dye tracer added to the salt solution was constant for all experiments. The slight deviations in photograph contrast are due to inherent variability in the film and film development process. Notable features are discussed in the text.

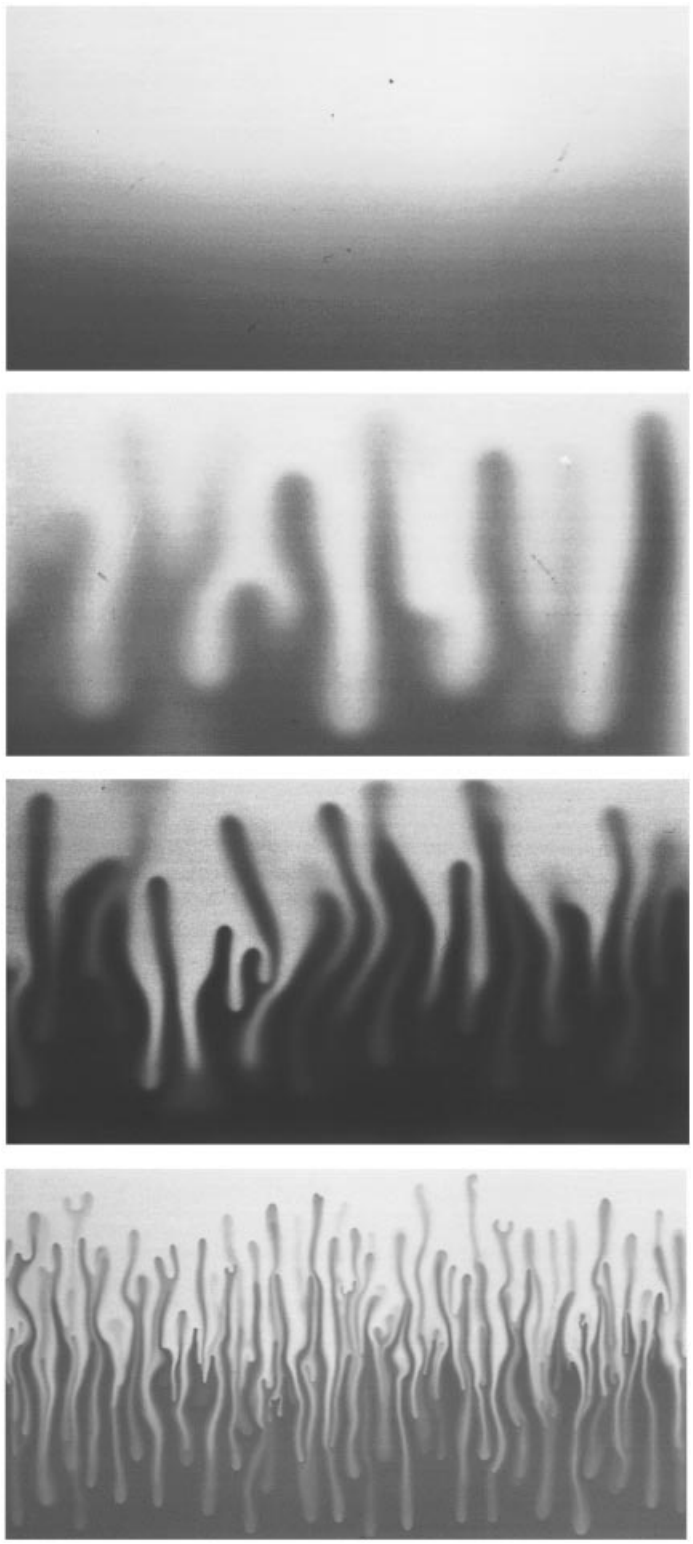

FIGURE 4 (*a–d*). For caption see facing page.

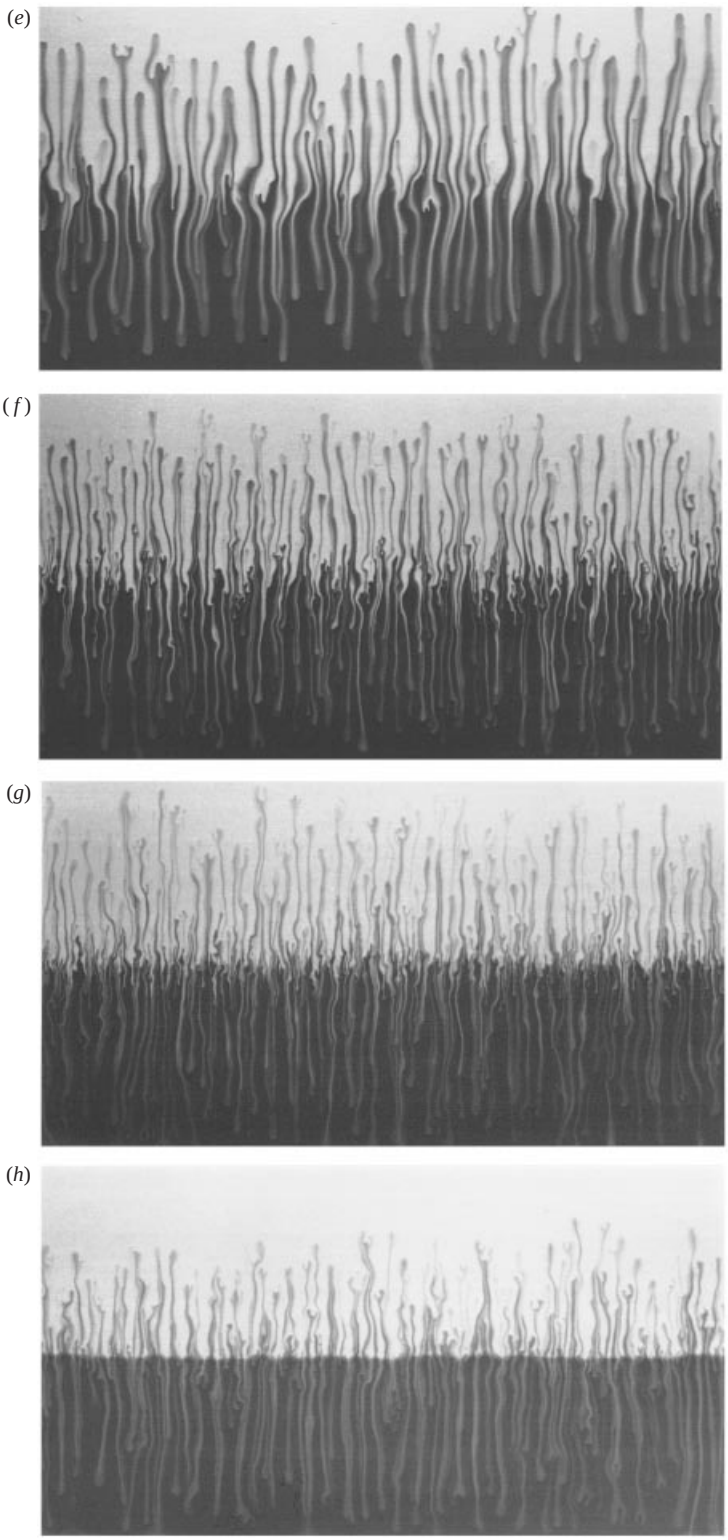

FIGURE 4 (*e–h*). For caption see page 170.

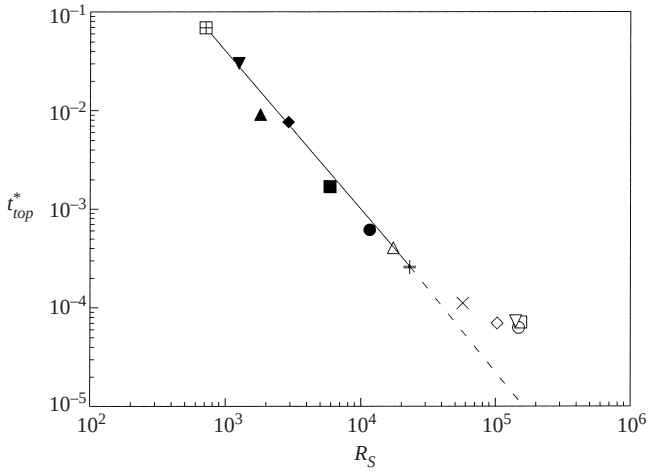

FIGURE 5. Dimensionless time, t^*_{top} ($= t_{top}D_T/H^2$), just prior to contact between the fastest convecting finger and either the top or bottom boundary for experiments 2 to 14, as a function of R_S. Behaviour follows an approximate power law for $700 < R_S < 2.29 \times 10^4$ (solid line) then deviates at higher R_S (dashed line). The 4 repeated runs of experiment 9 (+) show negligible variability in time required for the fastest convecting finger to reach the boundary.

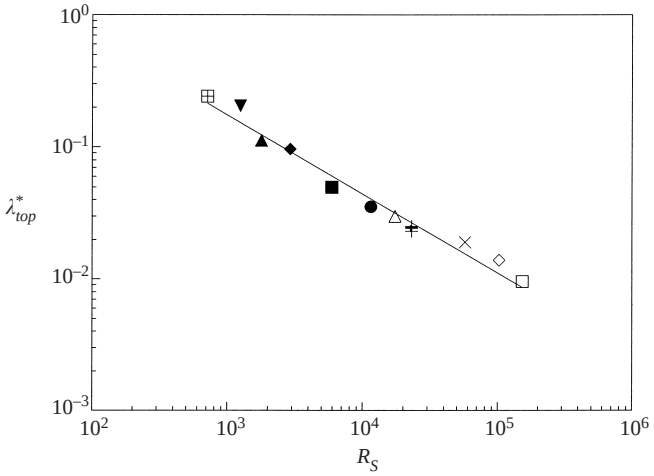

FIGURE 6. Dimensionless horizontal length scale, λ^*_{top} ($= \lambda_{top}/H$), just prior to contact between the fastest convecting finger and either the top or bottom boundary, for experiments 2 to 12, displays power law behaviour (solid line) as a function of R_S. The 4 repeated runs of experiment 9 (+) show a representative variability in the horizontal length scale of $\sim 3\%$.

(figures 4*b* and 4*c*) to narrow and sharp with thinner finger 'stems' feeding wider bulbous tips (figure 4*f–h*). Bulbous tips were observed in the salt finger experiments of Taylor & Veronis (1986) at large ΔS, and they also appear in the salt finger calculations of Shen (1989). At R_S above 1.15×10^4 (figure 4*d–h*) the bulbous finger tips themselves become unstable and generate additional finger pairs.

Figure 9 shows magnifications of a portion of the finger generation zone for experiments 9 to 14. Within the finger generation zone, the structural complexity gradually increases with R_S and reaches a peak at the apex R_S of 1.53×10^5 (figure 9*d*). At this peak, the continuous generation of new fingers at a scale nearly identical with

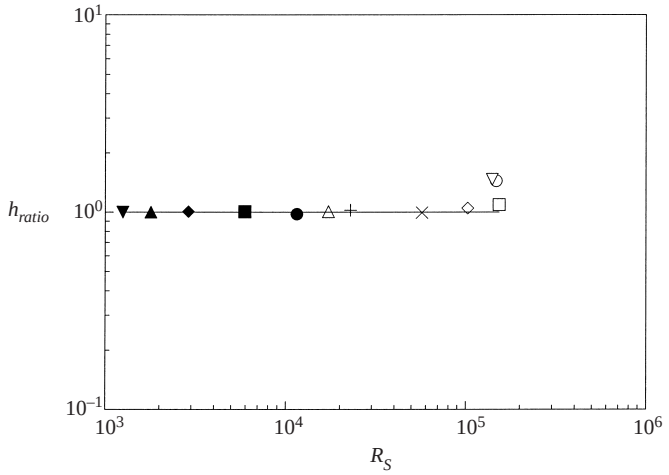

FIGURE 7. Characterization of flow symmetry, h_{ratio} ($= h_{descending}/h_{ascending}$), for experiments 3 to 14 as a function of R_S, where $h_{descending}$ is the height of the 10 fastest downward convecting fingers and $h_{ascending}$ is the height of the 10 fastest upward convecting fingers. The solid line indicates symmetric flow, $h_{ratio} = 1$.

the initial finger width causes an intense 'folding' and ramified structure that is probably fractal between this smallest length scale and the scale of the cell. At higher concentrations, as the salt solution approaches the solubility limit, complexity within the finger generation zone sharply decreases and the initial fluid interface remains distinct in time (figure 9*e*,*f*). Now, fingers tend to form at preferred locations that are maintained as the system evolves. Thus, the 'folding' that increases structure complexity along the assent to the apex R_S is suppressed in the descent, leading to very different convective structure.

4.2. *Vertical length scale growth*

We define the vertical length scale of the fingering region, h, as the average distance between the location of the tips of the 10 farthest advanced ascending and descending fingers. For each experiment, we measured a series of photographs (~ 6) from early time until the fastest convecting finger contacted either the top or bottom boundary. The vertical length scale, h^* ($= h/H$), in time, t^* ($= tD_T/H^2$), is shown in figure 10 for $1.25 \times 10^3 < R_S < 1.54 \times 10^5$ (experiments 3 to 14). The finger heights for experiments 1 and 2 were not measured owing to the difficulty in detection of the finger peaks. Although the results of experiments 3 and 4 show a fair amount of scatter, at R_S of 2.90×10^3 and above (experiments 5 to 14), we find $h^* \propto t^*$ yielding a constant characteristic vertical finger growth rate, V_c^*, for each experiment. Similar linear relationships have been reported by Stern & Turner (1969), Linden (1973) and Taylor & Veronis (1996) in large tanks, and by Imhoff & Green (1988) and Cooper *et al.* (2001) in porous media and a Hele-Shaw cell, respectively.

For relatively low Rayleigh numbers (experiments 3 and 4), the growth of h^* slows and then picks up again, as can be seen in figure 10 (solid triangles). Such a trend is also observed for double-diffusive convection in three-dimensional tanks, where it is attributed to large-scale circular convection in the upper and lower layers of the system (e.g. Taylor & Veronis 1996). There, the large-scale circular motions shear off the tips of the convecting fingers and limit their growth. However, in our Hele-Shaw cell experiments, large-scale circular convection did not occur; therefore, a different

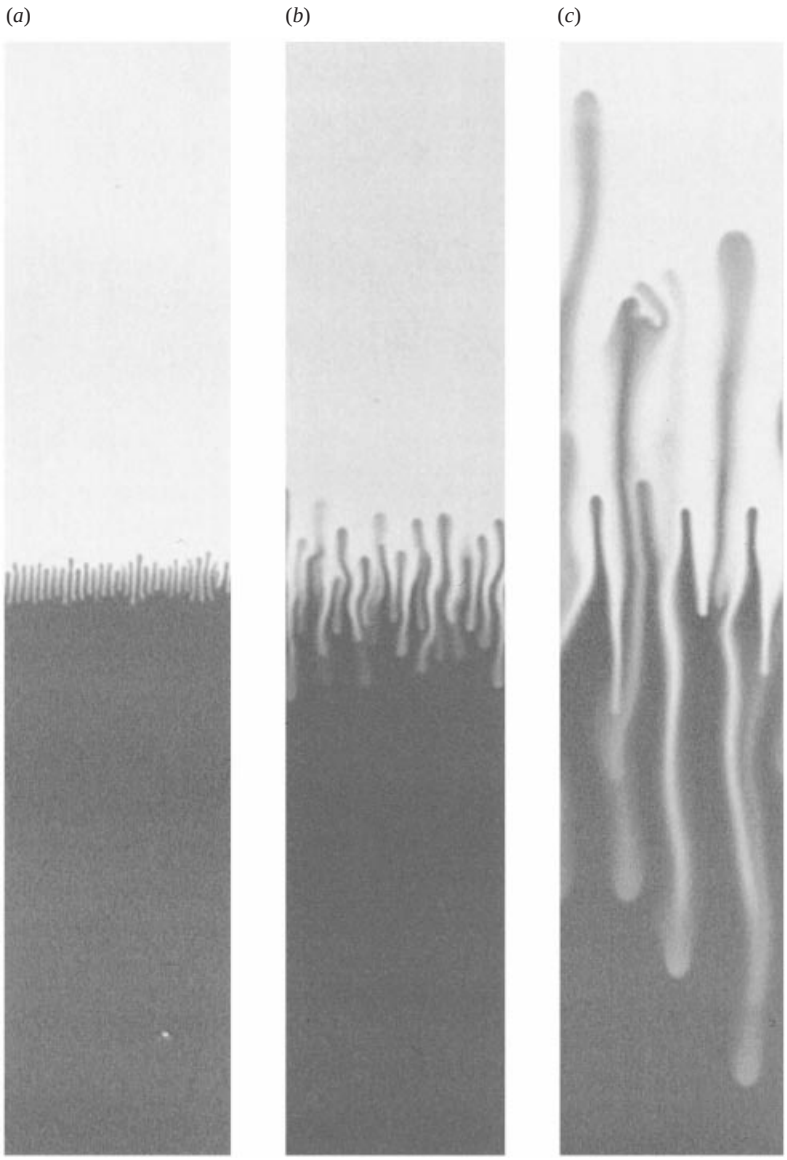

FIGURE 8. Representative regions ($\sim 3 \times 12\,\mathrm{cm}^2$) of the convective motion (light region indicates sucrose, dark region salt) for experiment 9 (R_S of 2.29×10^4) at (*a*) 4, (*b*) 16, and (*c*) 70 min. Notable features discussed in text.

mechanism acts to cause the reduction in growth at early time. For moderate to high Rayleigh numbers, early time behaviour is characterized by a relatively high finger frequency, and these small-scale fingers initially grow without influence from their neighbours. However, in time, fingers widen and thus begin to interact causing subsequent merger and the formation of a trunk structure where new finger pairs are continuously generated. This transition or reorganization is accompanied by minimum growth in the vertical direction and is consistent with the results of Shen & Veronis (1991) for numerical simulations of solute fingering in a Hele-Shaw cell. The dip in the vertical growth is not evident in our data (experiments 5 to 14) because

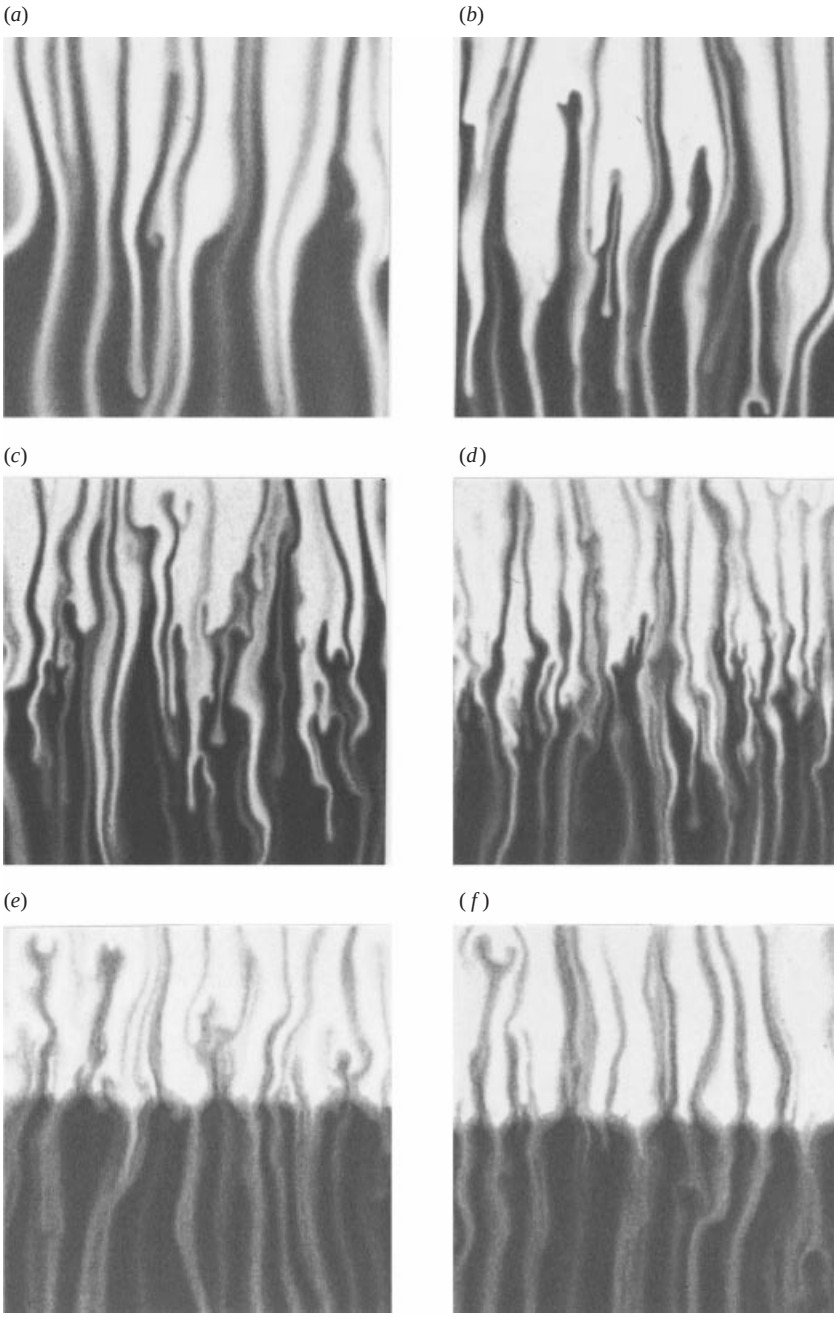

FIGURE 9. Representative regions ($\sim 4 \times 4\,\mathrm{cm}^2$) that capture the finger structure near the initial fluid interface for experiments 9 to 14(*a–f*). As concentrations increase, the structure becomes more complex (*a–d*) and then is suppressed causing the initial fluid interface to remain distinct (*e*,*f*).

the relatively large time increments chosen between photographs did not allow the growth rates of h^* to be determined at very early time, but it is probable that it also occurs for these experiments.

Another interesting result comes from considering the variation of the heights of

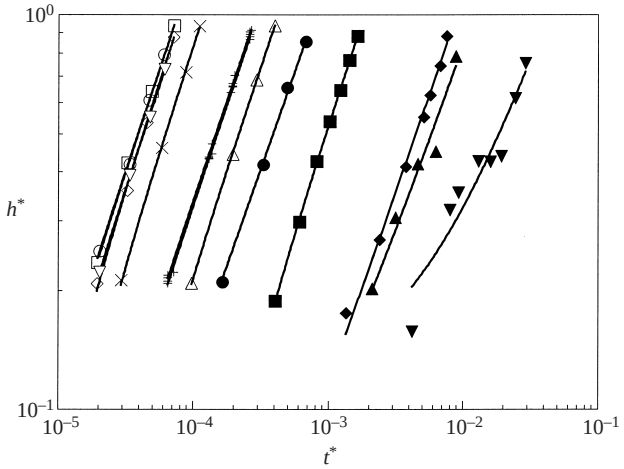

FIGURE 10. Dimensionless vertical length scale, h^* ($= h/H$), as a function of dimensionless time, t^* ($= tD_T/H^2$). Behaviour shows, in general, linear response (shown by regression lines); however, there are transition periods that appear in ▼, experiment 3 and ▲, experiment 4. The time to reach a given h^* decreases for each sequential experiment with the notable exception of experiments 11 to 14 (◇, 11; □, 12; ○, 13; ▽, 14) where the data show little variation. The 4 repeated runs of experiment 9 (+) show a representative variability in h^* of $\sim 1.5\%$.

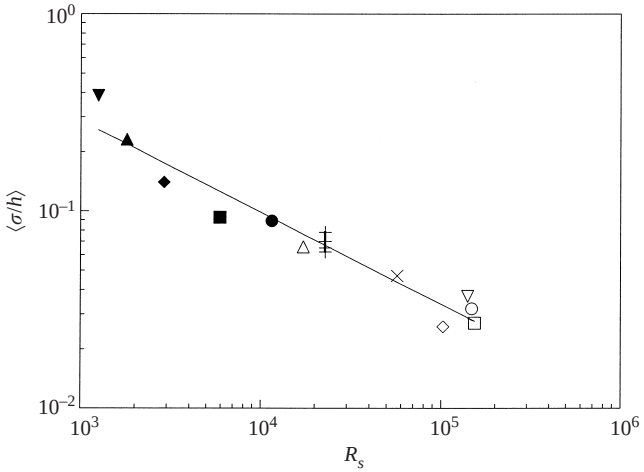

FIGURE 11. The average normalized standard deviation in the height of the measured fingers, $\langle\sigma/h\rangle$, as a function R_S shows a power law relationship (solid line). The 4 repeated runs of experiment 9 (+) show an average representative variability of $\sim 10\%$.

the fastest 10 ascending and 10 descending fingers. The normalized standard deviation in the measured finger heights, σ/h, does not show a significant trend in time within a single experiment. The average normalized standard deviation, $\langle\sigma/h\rangle$, across all measurements for a single experiment, decreases with R_S and obeys a power law with an exponent of -0.46 (figure 11). However, we note that this decrease in $\langle\sigma/h\rangle$ is also influenced by the increase in the number of fingers that each experiment contains. If we compare an R_S of $\sim 2.90 \times 10^3$ (figure 4*c*) with an R_S of $\sim 2.29 \times 10^4$ (figure 4*e*) and consider only a horizontal zone that contains the same number of fingers, $\langle\sigma/h\rangle$ for the higher R_S will increase. In other words, our measurement of only the 10

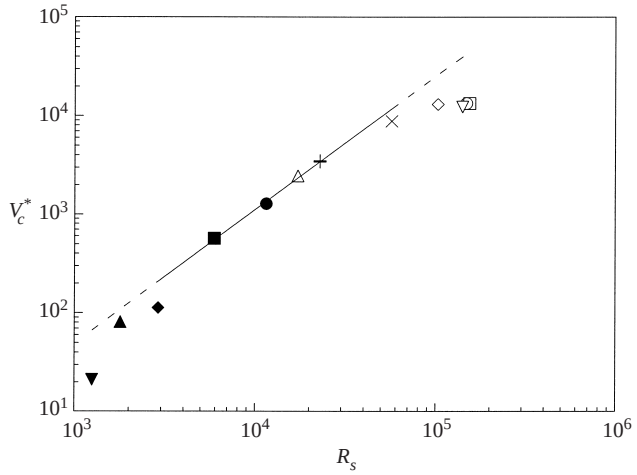

FIGURE 12. The dimensionless characteristic velocity, V_c^* ($= V_c H/D_T$), for the convecting fingers in experiments 3 to 14 as a function of R_S. At very dilute and concentrated solutions (dashed line) deviation from linearity is observed. The 4 repeated runs of experiment 9 (+) show an average representative variability of $\sim 1.5\%$.

fastest fingers in an experiment biases our measure of $\langle \sigma/h \rangle$ and could overpredict the absolute value of the exponent in the power law.

Figure 12 presents the dimensionless characteristic velocity, V_c^* ($= V_c H/D_T$), as a function of R_S. In the midrange, for $5.91 \times 10^3 < R_S < 2.29 \times 10^4$, V_c^* increases linearly due to the systematic increase in buoyant forces driving the motion. Above this range, for $R_S > 5.71 \times 10^4$, V_c^* approaches a constant value and, regardless of the Rayleigh number magnitude, the vertical growth rate is invariant. This behaviour, with nearly three orders of magnitude variation in V_c^* and the transition to the constant value at high concentration, emphasizes the strong variation of system behaviour at fixed R_ρ over the full concentration range.

4.3. *Horizontal length scale growth*

We define the horizontal length scale, λ, by dividing the cell width by half the number of transitions between dyed and un-dyed solutions along the initial fluid interface. The λ was not measured for experiments 1 and 2 because fingers were too diffuse, or for experiments 13 and 14 because it was difficult to detect finger edges with certainty because of the fineness of the convective structure. Figure 13 shows the temporal development of λ^* ($= \lambda/H$), for $1.25 \times 10^3 < R_S < 1.54 \times 10^5$ (experiments 3 to 12). Across the entire range, λ^* increases with time following a power law with exponent η. For the range of $1.25 \times 10^3 < R_S < 5.71 \times 10^4$ (experiments 3 to 10), $\eta = 0.54 \pm 0.03$, and for higher R_S, η begins to decline reaching a value of 0.1 at an R_S of 1.54×10^5 (experiment 12) (figure 14).

For dilute solutions, the numerical simulations of Shen & Veronis (1991) ($R_\rho = 1.5$ and 2.0, $\tau = 0.33$ (salt–sucrose), and $R_T = 2500$, which is similar to experiment 5 in the current work) reveal a power law relation with η of 0.5 (solid line in figure 14). Cooper *et al.* (2001) also report a constant value for η of ~ 0.5 for R_ρ ranging from 1.4 to 2.8 in salt–sucrose system experiments with salt concentrations comparable to the current experiments 5 to 8. However, for $R_S > 1.03 \times 10^5$ (experiments 11 and 12), the finger structure becomes more complex, yielding a slower increase in λ^* with time, and hence a decrease in η.

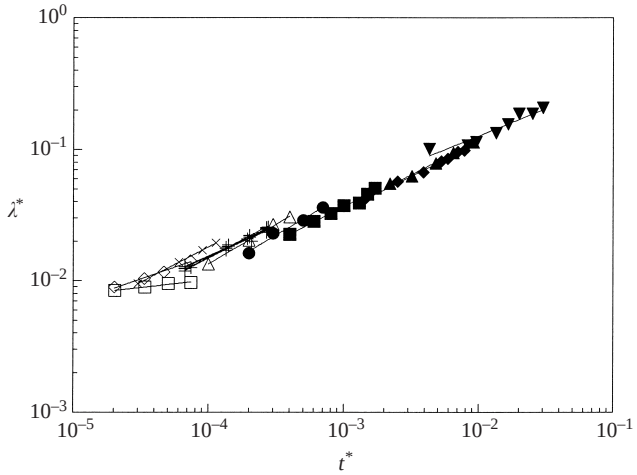

FIGURE 13. Dimensionless horizontal length scale, λ^* ($= \lambda/H$), as a function of dimensionless time, t^* ($= tD_T/H^2$), displays power law behaviour over the entire range. The 4 repeated runs of experiment 9 (+) show a representative variability of $\sim 3\%$.

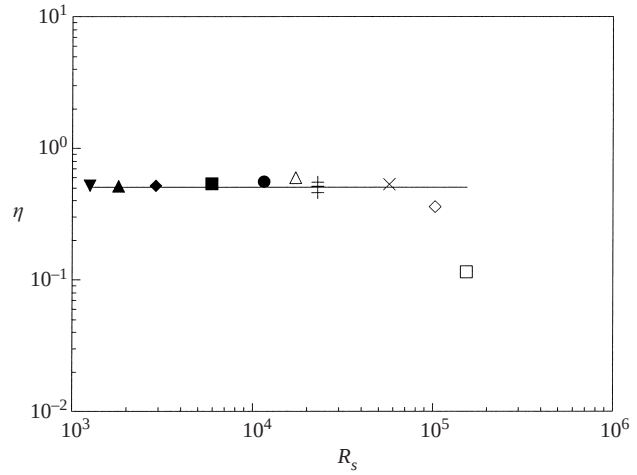

FIGURE 14. The power law exponent, η, obtained from the $\lambda^*(t^*)$ relationship as a function of R_S. The solid line represents a theoretical η equal to 0.5. The 4 repeated runs of experiment 9 (+) show an average representative variability of $\sim 8\%$.

Considering the early time horizontal length scale, λ^*_{early}, we see a general decrease with R_S of over an order of magnitude (figure 15). Linear stability analysis conducted by Nield & Bejan (1992) suggests the relationship $\lambda^*_{early} \propto R_S^{-0.5}$, shown by the solid line in figure 15. In the midrange, for $5.91 \times 10^3 < R_S < 2.29 \times 10^4$, the experimental results and theory correlate reasonably well. However, at low R_S, we again see some scatter, and for $R_S > 5.71 \times 10^4$, λ^*_{early} levels off and approaches a constant value.

4.4. *Discussion of deviations at high concentration*

In the range of Rayleigh space up to $R_S = 5.71 \times 10^4$ (experiments 1 to 10), the dilute approximation holds along with equations (3) to (5), and we see systematic changes in behaviour as a function of R_S for fixed R_ρ. Behaviour is found to be reasonably well represented with $h_{ratio} = 1$, $V_c^* \propto R_S$, $\eta \cong 0.5$, and $\lambda^*_{early} \propto R_S^{-0.5}$. In the high

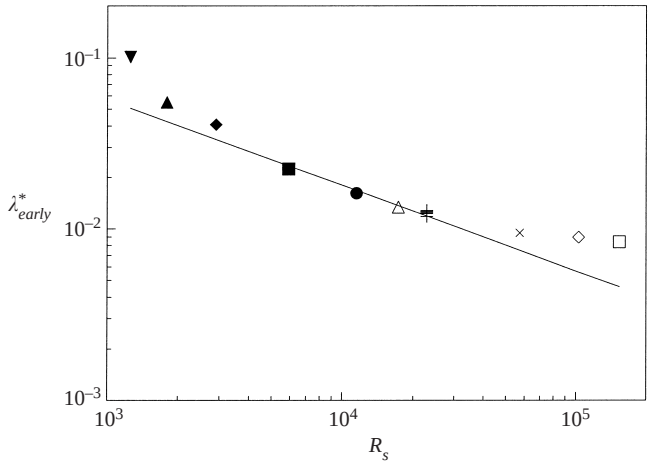

FIGURE 15. Dimensionless horizontal length scale at early time, λ^*_{early} ($= \lambda_{early}/H$), as a function of R_S. λ^*_{early} is taken as the first point measured for each experiment, as shown in figure 13. The solid line gives the theoretical relationship predicted by linear stability analysis with exponent of -0.5 (Nield & Bejan 1992). The 4 repeated runs of experiment 9 (+) show an average representative variability of $\sim 6\%$.

R_S region ($R_S > 1.03 \times 10^5$, experiments 11 and higher), the component diffusion coefficients, chemical expansion coefficients and fluid viscosities all vary significantly within the problem domain owing to their dependency on solute concentration, and as concentrations go beyond dilute, the momentum (3) and advection–diffusion equations (4) and (5) become nonlinear. In this realm, the prior definitions of dimensionless parameters do not properly represent system behaviour.

To examine the asymmetric growth between the upward and downward moving fingers at high concentration, we consider the influence of differential solution viscosity such as suggested by Imhoff & Green (1988). Redefining each Rayleigh number to reflect the viscosity of each corresponding solution, we can rewrite (11) as

$$R_\rho = \frac{\hat{R}_T}{\gamma \hat{R}_S} = \frac{\beta_T \Delta T}{\beta_S \Delta S}, \tag{14}$$

where $\hat{R}_T = \beta_T \Delta T g H k / D_T \nu_T$, $\hat{R}_S = \beta_S \Delta S g H k / D_T \nu_S$, and the additional dimensionless viscosity ratio, $\gamma = \nu_S / \nu_T$, arises as part of our problem. Note that, of course, the product $\gamma \hat{R}_S$ is linear with $\hat{R}_T$ for a fixed R_ρ. The ratio of descending to ascending finger heights as a function of the viscosity difference is linear with γ (figure 16). Additionally, we see that the viscosity of the solution into which the fingers move, rather than the viscosity of the fingers themselves, plays the critical role in determining their velocity, i.e. fingers move slower into the sucrose solution than the salt solution.

The simple linear $V_c^* \propto R_S$ relationship can also be extended for high solute concentrations by considering $V_c^* \propto \hat{R}_S$ (figure 17). Additionally, if we recognize that our R_ρ values for experiments 11, 13 and 14 deviate from our target value of 1.083 more than any other experimental points, we can consider the added influence of the stabilizing (salt) solution that decreases the buoyant drive and write

$$V_c^* \propto \hat{R}_S (R_\rho + 1) \tag{15}$$

from a simple scale analysis. Recognizing that R_ρ is negative, we see that the small deviation ($\sim 1\%$) from our target R_ρ value for these experiments corresponds to

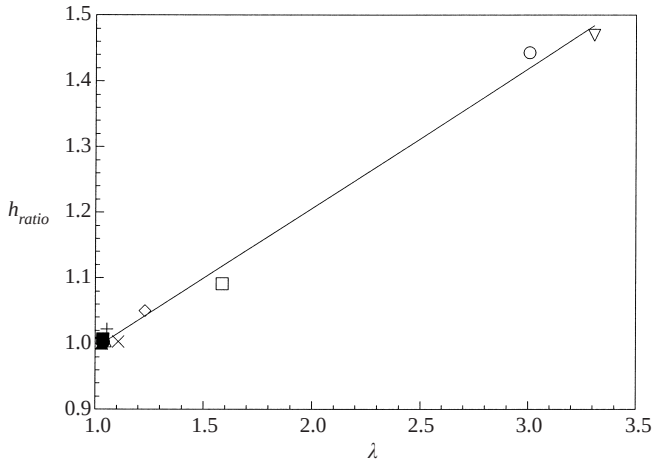

FIGURE 16. Characterization of flow symmetry, h_{ratio} ($= h_{descending}/h_{ascending}$), as a function of $\gamma(= v_S/v_T)$. Linear regression of the data given as the solid line.

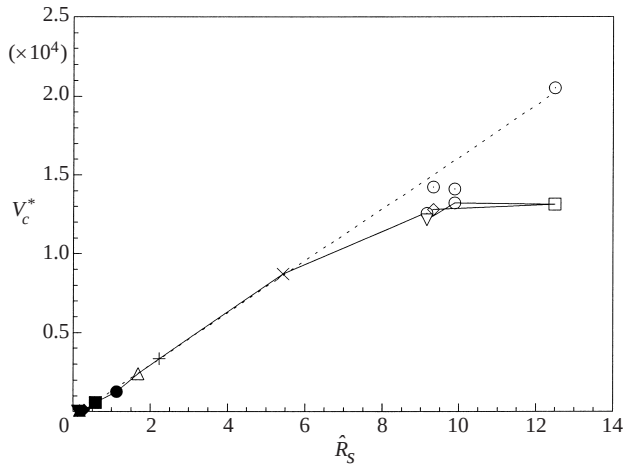

FIGURE 17. Comparison of the relationship $V_c^* \propto \hat{R}_S$ (dashed line) to data (solid line) shows a good match at low and a reasonable match at high concentration. Considering the variation from the target R_ρ (equation 16) for experiments 11, 13 and 14, we see an improved correspondence at high concentrations (⊙). However, for □, experiment 12 where the most complex finger structure emerged, equation (15) does not predict V_c^* well.

$\sim$ 15% change in the magnitude of V_c^*. Replotting these three experimental points using the actual R_ρ for each experiment shows (15) to perform well at high concentrations (figure 17, dotted circles). However, (15) is still off in the midrange on the assent up the R_ρ spoke (experiment 11, open diamond compared to dotted circle for $\hat{R}_S$ of 9.32×10^4) and far overpredicts the velocity at the apex (experiment 12, open square compared to dotted circle for $\hat{R}_S$ of 1.25×10^5). In both of these experiments we see increased structural complexity within the finger generation zone, especially at the apex (figure 4*g*), and thus we believe additional energy dissipation mechanisms must be operating such as to result in the observed discrepancy with (15).

With respect to λ^* at early time and its successive growth, we find that for

$R_S > 1.03 \times 10^5$ (experiments 11 and 12), λ^* starts off smaller and grows slower than suggested by extrapolation from dilute behaviour where $\lambda^*_{early} \propto R_S^{-0.5}$ and $\eta \cong 0.5$. Over the range encompassed by experiments up to and including 12, incorporation of γ into the exponent can capture behavioural trends reasonably well (e.g. $\eta = 0.54/\gamma^{3.8}$). However, we note that for highly concentrated solutions where we see the most extreme deviations in behaviour (experiments 13 and 14), we could not measure the horizontal length scale with reasonable certainty. There, the increase in γ stabilizes the initial fluid interface with respect to finger pair generation such that the structural complexity present in experiments 11 and 12 is suppressed. We note, however, that this suppression may not be a simple function of γ at these high concentrations as τ, β_T and β_S all decrease, and the salt and sucrose may additionally interact to influence both viscous and diffusive processes.

5. Conclusion

Double-diffusive finger convection in a salt–sucrose system was studied at fixed R_ρ with systematic increase in solution concentration. Our results in a Hele-Shaw cell demonstrate that at low concentrations, observed behaviour requires only two of the three parameters R_ρ, R_T and R_S to be specified. However, as concentrations increase, the specifics of the chemical interactions become important. For the salt–sucrose system, near the Rayleigh number apex, the component diffusion coefficients, chemical expansion coefficients and fluid viscosities all begin to vary within the problem domain. For these high concentrations, at least the dimensionless viscosity ratio, $\gamma = \nu_S/\nu_T$, must also be included to describe behaviour. In order to conduct a more comprehensive study, experimental measurements of full concentration fields using non-intrusive methods (e.g. Cooper *et al.* 2001) are required. Such data would allow us to test hypothesized component flux relations (e.g. Turner 1973) as well as to both develop and test new numerical simulation approaches (e.g. Stockman *et al.* 1998). In closing, we mention that the behaviour of highly concentrated double-diffusive systems is probably of importance in the fields of metallurgy, material science, and geophysics where the solutions of interest are often concentrated melts in problems as diverse as controlled crystal growth and magma convection.

Financial support for this research was provided by the US Department of Energy's Basic Energy Sciences Geoscience Program under contract DE-AC04-94AL85000. Experiments were conducted in the Flow Visualization and Processes Laboratory at Sandia National Laboratories. We thank the three anonymous reviewers for their insightful comments and careful reviews of the manuscript. We thank Bruce Thomson and Clay Cooper for their contribution to discussions concerning this topic. We also thank Mark Haaganstad for his assistance with the experiments and in the construction of the Hele-Shaw cell, and Anthony Chavez for his expertise in cell fabrication.

REFERENCES

Azouni, M. A. 1981 Time-dependent natural convection in crystal growth systems. *PhysicoChem. Hydrodyn.* **2**, 295–309.

Cooper, C. A., Glass, R. J. & Tyler, S. W. 1997 Experimental investigation of the stability boundary for double-diffusive finger convection in a Hele-Shaw cell. *Water Resour. Res.* **33**, 517–526.

Cooper, C. A., Glass, R. J. & Tyler, S. W. 2001 Affect of buoyancy ratio on the development of double-diffusive finger convection in a Hele-Shaw Cell. *Water Resour. Res.* **37**, 2323–2332.

Dalziel, S. B., Linden, P. F. & Youngs, D. L. 1999 Self-similarity and internal structure of turbulence induced by Rayleigh–Taylor instability. *J. Fluid Mech.* **399**, 1–48.

Detwiler, R. L., Rajaram, H. & Glass, R. J. 2000 An investigation of the relative importance of Taylor dispersion and macrodispersion in variable aperture fractures. *Water Resour. Res.* **36**, 1611–1625.

Fisher, K. M. 1981 The effects of fluid flow on the solidification of industrial castings and ingots. *PhysicoChem. Hydrodyn.* **2**, 311–326.

Green, T. 1984 Scales of double-diffusive fingering in porous media. *Water Resour. Res.* **20**, 1225–1229.

Gregg, M. C. 1973 The microstructure of the ocean. *Sci. Am.* **228**, 65–77.

Imhoff, P. T. & Green, T. 1988 Experimental investigation of double-diffusive groundwater fingers. *J. Fluid Mech.* **188**, 363–382.

Irani, R. R. & Adamson, W. 1958 Transport processes in binary liquid systems. I. Diffusion in the sucrose–water system at 25°. *J. Phys. Chem.* **62**, 1517–1521.

Langer, J. S. 1980 Instabilities and pattern formation in crystal growth. *Rev. Mod. Phys.* **52**, 1–28.

Linden, P. F. 1973 On the structure of salt fingers. *Deep Sea Res.* **20**, 325–340.

Linden, P. F., Redondo, J. M. & Youngs, D. L. 1994 Molecular mixing in Rayleigh–Taylor instability. *J. Fluid Mech.* **265**, 97–124.

Loper, D. E. & Roberts, P. H. 1983 Compositional convection and the gravitationally powered dynamo. In *Stellar and Planetary Magnetism* (ed. A. M. Soward), pp. 297–327.

Nield, D. A. 1968 Onset of thermohaline convection in porous medium. *Water Resour. Res.* **4**, 553–560.

Nield, D. A. & Bejan, A. 1992 *Convection in Porous Media.* Springer.

Proctor, M. R. E. & Weiss, N. O. 1982 Magneto-convection. *Rep. Prog. Phys.* **45**, 1317–1379.

Schmitt, R. W. 1994 Double-diffusion in oceanography. *Annu. Rev. Fluid Mech.* **26**, 255–285.

Shen, C. Y. 1989 The evolution of the double-diffusive instability: salt fingers. *Phys. Fluids* A **5**, 829–844.

Shen, C. Y. 1995 Equilibrium salt-fingering convection. *Phys. Fluids* **7**, 706–717.

Shen, C. Y. & Veronis, G. 1991 Scale transition of double-diffusive finger cells. *Phys. Fluids* A **3**, 58–68.

Shen, C. Y. & Veronis, G. 1997 Numerical simulation of two-dimensional salt fingers. *J. Geophys. Res.* **102**, 23 131–12 143.

Spiegel, E. A. 1972 Convection in stars. II. Special effects. *Annu. Rev. Astron. Astrophys.* **10**, 261–304.

Stern, M. E. 1975 *Ocean Circulation Physics.* Academic.

Stern, M. E. & Turner, J. S. 1969 Salt fingers and convecting layers. *Deep-Sea Res.* **16**, 497–511.

Stockman, H. W., Glass, R. J., Cooper, C. & Rajaram, H. 1998 Accuracy and computational efficiency in 3D dispersion via lattice-Boltzmann: models for dispersion in rough fractures and double-diffusive convection. *Intl J. Mod. Phys.* C **9**, 1545–1557.

Stokes, R. H. 1950 The diffusion coefficients of eight univalent electrolytes in aqueous solution at 25°. *J. Am. Chem. Soc.* **72**, 2243–2247.

Taylor, J. & Veronis, G. 1986 Experiments on salt fingers in a Hele-Shaw cell. *Science* **231**, 39–41.

Taylor, J. & Veronis, G. 1996 Experiments on double-diffusive sugar–salt fingers at high stability ratio. *J. Fluid Mech.* **321**, 315–333.

Turner, J. S. 1973 *Buoyancy Effects in Fluids.* Cambridge University Press.

Turner, J. S. 1985 Multicomponent convection. *Annu. Rev. Fluid Mech.* **17**, 11–44.

Weast, R. C. (ed.) 1986 *CRC Handbook of Chemistry and Physics*, 66th edn. CRC Press, Boca Raton, FL.

Wooding, R. A. 1969 Growth of fingers at an unstable diffusing interface in a porous medium or Hele-Shaw cell. *J. Fluid Mech.* **39**, 477–495.